Journal of Materials Chemistry A

Accepted Manuscript

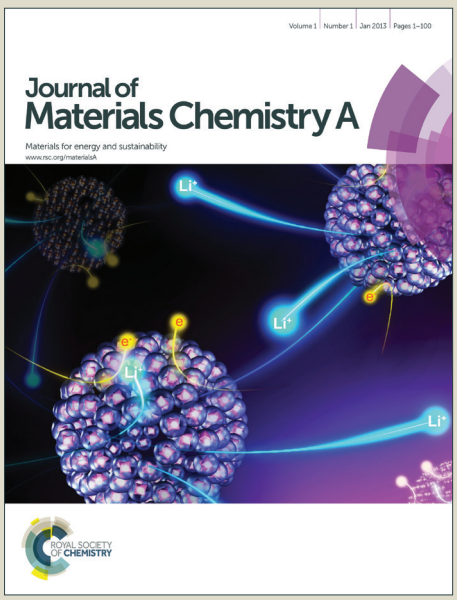

ROYAL SOCIETY OF CHEMISTRY

www.rsc.org/materialsA

Layered Inorganic-Organic Hybrid Material Based on Reduced Graphene Oxide and α-$Ni(OH)_2$ for High Performance Supercapacitor Electrodes

Sourav Bag and C. Retna Raj*

Functional Materials and Electrochemistry Laboratory
Department of Chemistry
IIT Kharagpur
Kharagpur 721302, West Bengal, India

E-mail: crraj@chem.iitkgp.ernet.in

Abstract

A facile one-step strategy for the synthesis of novel layered hybrid material of reduced graphene oxide (rGO) and α-$Ni(OH)_2$ by non-hydrothermal route and the supercapacitive performance of the material are described. The hybrid material rGO/α-$Ni(OH)_2$ was synthesized using glucose as a templating agent for the growth of layered α-$Ni(OH)_2$ and a reducing agent for the reduction of graphene oxide (GO). The templating agent partially reduces GO to rGO and assist the growth of α-$Ni(OH)_2$ layers in between the rGO sheets. The electron microscopic measurements shows the stacking of layered α-$Ni(OH)_2$ over rGO sheets. The activity of the hybrid material was evaluated by voltammetric, electrochemical impedance and charge-discharge measurements in alkaline pH in terms of specific capacitance, internal resistance and capacitance retention. The hybrid material has superior performance compared to rGO, free α-$Ni(OH)_2$ and the physical mixture of rGO and free α-$Ni(OH)_2$. High specific capacitance of 1671.67 Fg^{-1} was obtained at the current density of 1A g^{-1}. The hybrid material retains 81% of its initial capacitance after 2000 continuous charge-discharge cycles. The large surface area and high electronic conductivity of the hybrid material favor a facile charge transport whereas the layer structure of assures the easy diffusion of electrolytes ions and enhances the overall performance. Asymmetric supercapacitor device was made by pairing the hybrid material with rGO and it delivers high energy density of 42.67Wh/kg at the power density of 0.4kW/kg.

Introduction

The depletion of fossil fuels, increase in the energy requirement and the growing concern over the environmental consequences of the use of fossil fuels demand for alternative efficient, green and renewable energy sources. The renewable sources like the sun and wind are very promising and the electricity generated from these sources can meet the future energy requirements. However, appropriate energy storage technology is required to store the electricity generated from these renewable sources. The US Department of Energy gives equal emphasis for both supercapacitors and batteries as potential future energy storage devices.[1] Supercapacitors have received significant interest as they offer high power density and long cycle life with respect to batteries and electric double layer capacitors.[2] Supercapacitors bridge the gap between batteries and conventional capacitors and they are ideal for portable electronics and automobiles where fast and high power delivery is required.[2] The properties of the electrode material actually decide the overall performance of the supercapacitors. Several efforts have been taken in the past to develop materials that are capable of delivering high energy density and having excellent recyclability. The traditional materials such as carbon, redox polymers, metal oxides and hydroxides, etc. have been used in the past for the development of supercapcitors.[3-6] For instances, the transition metal oxides such as, MnO_2, RuO_2, Co_3O_4, $Ni(OH)_2$, etc. have been explored as a pseudocapacitive materials to achieve high specific capacitance and energy density.[7] However, significant improvement in the performance of these materials is necessary to meet the requirement of portable electronics, hybrid electric vehicles, etc. One of the major concerns with the transition metal oxide and hydroxide based materials is the poor recyclability, presumably due to the insulating nature of the material.

The integration of transition metal oxides with highly conductive carbon materials such as carbon nanotube, graphene, etc. can circumvent problems associated with the rate

capability and sluggish charge transport.[8] The synthesis of composite materials of transition metal oxides and two dimensional honeycomb carbon network, graphene, is a promising approach in the development of supercapcitors.[5] The one atom thick graphene has large surface area, excellent electrical conductivity, high mechanical strength and flexibility.[4, 9-10] The intrinsic properties of graphene made it an excellent candidate for various electronic applications. The composite materials derived from transition metal oxides and graphene/reduced graphene oxide (rGO) would be an ideal choice for the development of energy conversion and storage devices. In the recent past, the composite materials derived from rGO and metal oxides such as, Co_3O_4, $NiFe_2O_4$, $NiCo_2O_4$, etc. have been used for supercapacitor applications.[11-15] Specific capacitance ranging from 111 to 737 Fg^{-1} has been achieved with these composite materials.[11-15] $Ni(OH)_2$ is one of the promising inexpensive material for supercapacitor applications as it has high theoretical specific capacitance of 2082 Fg^{-1} and has layer structure with large interlayer distance.[5] $Ni(OH)_2$ exists in two different phases (α and β); the α-$Ni(OH)_2$ has layer structure with intercalated water molecules in between the layers. Although several reports describe the supercapacitive performance of β phase, only limited studies have been performed with the α phase. Recently, the composite material of $Ni(OH)_2$ and rGO/carbon nanotubes has been exploited for supercapacitor applications.[16] Specific capacitance in the range of 215-1828 F g^{-1}, depending on the current density, has been achieved.[17-22] It has been shown that the supercapacitive performance of graphene-$Ni(OH)_2$ material is significantly better than the free $Ni(OH)_2$.[23, 24]

The inorganic-organic hybrid materials with layer structure can be of immense interest in the development of biosensing and energy storage devices.[25, 26] Stacking of layered pseudocapacitive metal oxide such as $Ni(OH)_2$ in between rGO sheets can significantly improve the capacitive performance of the layered oxide materials. The layer-by-layer stacked materials have several advantages over the conventional composites materials. (i)

Enhanced accessibility of the electrode materials and decrease in the diffusion length of the electrolyte can significantly improve the capacitive performance. (ii) The large surface area of rGO sheets stacked in between the pseudocapacitive oxide material can offer electrochemical double layer capacitance. (iii) High capacitive retention can be achieved due to the confinement of the pseudocapacitive materials over rGO sheets.[27] It is an interesting approach to synthesize stacked hybrid material of rGO and $Ni(OH)_2$ for supercapacitor application. Herein, we describe a facile route for the synthesis of alternatively stacked layered hybrid material of rGO and α-$Ni(OH)_2$ using glucose as template and its supercapacitive performance. To the best of our knowledge, this is the first report on the synthesis of layered hybrid material of rGO and α-$Ni(OH)_2$.

Materials and Method

Graphite powder and polyvinylidene fluoride (PVF) were obtained from Sigma-Aldrich. All other chemicals used in this investigation were of analytical grade and obtained from Merck, India. All the solutions were prepared with Millipore water (Milli Q system).

Synthesis of GO

Modified Hummer's method was used to synthesize GO by the exfoliation of graphite.[28] In a typical procedure, graphite (1 g) and $NaNO_3$ (1 g) were taken in a round bottom flask and H_2SO_4 (50 mL) was slowly added to the mixture at 0 ^oC. Then solid $KMnO_4$ (6 g) was added to the reaction mixture and stirred continuously for an hour; water (200 mL) was added to the flask while stirring the mixture. Then H_2O_2 solution (5 mL, 30%) was added to the mixture until the gas evolution was ceased. The mixture was centrifuged in an ultra centrifuge and the yellow-brown solid was collected and dried under vacuum.

Synthesis of rGO/α-Ni(OH)$_2$ hybrid material

The layered hybrid material of rGO/α-Ni(OH)$_2$ was synthesized in aqueous solution according to the following procedure. Typically, GO (10 mg) was dispersed in 50 mL water by sonication in a round bottom flask for an hour. An aqueous solution of $Ni(NO_3)_3.6H_2O$ (7.5 mg/ mL) was then added to GO suspension and the mixture was stirred in a magnetic stirrer for 30 min. D-glucose (300 mg) was subsequently added to the mixture and stirred for another 30 min. Ammonia (50 µL of 25% w/w) was then added dropwise to the mixture and refluxed for 3 h under stirring in an oil bath at a temperature of 95 ^{o}C. The reaction mixture turned to black while refluxing and the product was filtered and washed extensively with copious amount of water and freeze dried. The free α-Ni(OH)$_2$ was synthesized with the identical procedure in the absence of rGO.

Instrumentation

Transmission electron microscopic (TEM) measurements were performed with JEOL JEM 2010 electron microscope operating at a voltage of 200 kV. Field emission scanning electron microscopic (FESEM) analysis was performed using Carl Zeiss Supra 40 and line scale mapping analysis was carried out with Oxford analytical instruments attached to the FESEM instrument. X-ray diffraction (XRD) profiles were acquired with BRUKER D8 advance unit using Cu-kα (λ=1.54Å) radiation. Fourier transform infrared (FTIR) spectroscopic measurements were performed with Perkin Elmer spectrophotometer RX1. Perkin Elmer Pyris Diamond TGA-DTA was used for the thermogravimetric analysis (TGA) of the samples. The analysis was performed at a temperature ramp of 10 ^{O}C/min. The X-ray photoelectron spectroscopic (XPS) measurements were carried out with PHI 5000 versaprobe II scanning XPS microscope using the energy source Al (Kα, hν = 1486.6 eV). Raman spectroscopic measurement was performed using a Jobin Yvon Horiba T64000 spectrometer

(France) with an excitation source of Argon Krypton mixed ion gas laser (514 nm, Spectra Physics, USA). Conductivity measurement was carried out using Keithley electrometer (model no 6514). All the electrochemical experiments were performed with Autolab potentiostat galvanostat (302N) in a single compartment three electrode electrochemical cell with saturated calomel as a reference and Pt foil as counter electrodes.

Electrode preparation

The working electrode was prepared by mixing hybrid material (80%) with acetylene black (15%) and polyvinylidene fluoride (PVF) (5%) dissolved in N-methyl-2-pyrrolidone (NMP) in a mortar pestle. The thus obtained slurry was then uniformly coated on nickel foam. The hybrid material coated nickel foam was then dried in vacuum oven at 60 ^{o}C for 12 h. The loading of the hybrid material was optimized and high specific capacitance was obtained at the loading of 1 mg cm^{-2}. The physical mixture of rGO and α-Ni(OH)$_2$ was obtained by mixing 1:10 ratio of the rGO and α-Ni(OH)$_2$. The loading of free α-Ni(OH)$_2$ and the physical mixture was also maintained at 1 mg cm^{-2}. All electrochemical experiments were performed under inert atmosphere and KOH (1 M) was used as an electrolyte. For the post mortem TEM and XRD analysis, the hybrid material was carefully removed from the current collector after extensive charge-discharge cycles. For TEM measurement, the material was first dispersed in methanol and aliquot of the dispersion was coated on the carbon coated copper grid and subjected to TEM measurement. Powder sample was used in the XRD analysis.

Result and Discussion

Synthesis and characterization of rGO/α-Ni(OH)$_2$

The hybrid material was synthesized according to Scheme 1 using glucose as template. The growth of α-Ni(OH)$_2$ over rGO involves the initial binding of Ni(II) ions and glucose with GO by electrostatic and hydrogen bonding interactions. Glucose plays two important roles as

(i) template for the growth of α-$Ni(OH)_2$ and (ii) reducing agent for the reduction of GO in ammonia solution. It is well known that GO sheets have abundant of oxygen containing functionalities such as carboxylate, carbonyl, hydroxyl and epoxide on both the sides. In solution, the electrostatic repulsion between the sheets essentially separates them from aggregation. The Ni(II) ions electrostatically bind with carboxylate groups of the GO sheets whereas the glucose molecules bind on the surface of the GO by hydrogen bonding interaction. Such hydrogen bonding interaction of glucose can sandwich two GO sheets together. The surface-bound glucose reduces GO to rGO in ammonia solutions.[29, 30] During the deoxygenation process, glucose was converted into gluconic acid, which complexes with Ni(II) ions. The Ni(II) ions are known to complex with gluconic acid in neutral to alkaline condition.[31,32] One would expect that the Ni(II) ions can freely diffuse away from GO surface due to lack of Ni(II) binding sites once the deoxygenation is complete. However, the complexation of Ni(II) with the in situ generated gluconic acid and excess glucose which are hydrogen bonded with rGO can confine the Ni(II) ions on GO surface. Moreover, the FTIR spectral measurements (Figure S1) shows that GO is not completely reduced during reaction, suggesting that Ni(II) can still have possible electrostatic interaction with the unreduced carboxylate groups. The thus surface-bound Ni(II) ions were further converted into α-$Ni(OH)_2$ while refluxing.

Figure 1 displays the XRD and Raman spectral profiles of GO, free α-$Ni(OH)_2$, and rGO/α-$Ni(OH)_2$ hybrid material. The peak at 10.35^o for GO corresponds to the interplanar distance (002 plane) of 0.85 nm. The peaks at (001), (110), (002) and (300) for attributed to the α phase of $Ni(OH)_2$ (JCPDS card no. 22-0444). The rGO/α-$Ni(OH)_2$ shows all the characteristic signature for α-$Ni(OH)_2$ along with a less intense broad peak in between 22^o and 24^o, corresponding to the (002) plan of rGO. The diffraction peak of (001) and (002) planes for the hybrid material is shifted to lower angle, possibly due to the stacking of

$Ni(OH)_2$ layers in between the rGO sheets. The diffraction profile is indexed to the rhombohedral phase of α-$Ni(OH)_2$ with lattice parameter a=b=5.15 and c = 9.96 Å. The interlayer spacing was calculated to be 0.99 nm, which is significantly higher than the free α-$Ni(OH)_2$ (0.78 nm). Such increase in the interlayer spacing confirms the stacking of α-$Ni(OH)_2$ layers over rGO sheets. The diffraction pattern for rGO is not seen in the profile, probably due to the non-uniform stacking of the layers. The Raman spectra for rGO/α-$Ni(OH)_2$ presented in Figure 1B shows the signature for both α-$Ni(OH)_2$ and rGO, further confirming the growth of α-$Ni(OH)_2$ and the partial reduction of GO. Both α-$Ni(OH)_2$ and rGO/α-$Ni(OH)_2$ shows the characteristic bands for the lattice modes of α-$Ni(OH)_2$ at 465 and 533 cm^{-1}.[33,34] These bands are ascribed to the symmetric Ni-OH stretching and Ni-O vibrational stretching modes.[33] Raman spectrum of GO shows D band at 1365 cm^{-1} corresponding to structural deformities of sp^2 domains due to oxygen functionalities. The G band corresponding to the first order scattering of E_{2g} mode was observed at 1610 cm^{-1}. The close examination of the intensity of these bands shows that the ratio I_D/I_G for rGO/α-$Ni(OH)_2$ is higher than GO suggesting the decrease in the size of sp^2 domain after the reduction of exfoliated GO and the existence of defects on the carbon network.[35] The FTIR measurements further support the reduction of GO and the growth of $Ni(OH)_2$ (Figure S1).

The XPS survey scan spectrum of the hybrid material shows the characteristic signature for carbon, oxygen and nickel (Figure 2A). The 2p region of nickel has two major peaks at 855.1 and 873.3 eV corresponding to Ni $2p_{3/2}$ and Ni $2p_{1/2}$, respectively, with a spin-energy separation of ~18 eV, which is in close agreement with the earlier literature for $Ni(OH)_2$.[21] The satellite peaks corresponding to the Ni $2p_{3/2}$ and Ni $2p_{1/2}$ were observed at 861.2 and 879.4 eV.[36] The deconvoluted C1s signal for GO has two main peaks centred at 284.4 and 286.5 eV associated with the sp^2 C-C and C-O bonds, respectively. The peak at 288.6 eV corresponds to the C=O and O-C=O bonds of oxygen containing functionalities on

GO surface. The decrease in the intensity of the peaks at 286.5 and 288.6 eV and the enhancement in the intensity of the peak at 284.4 eV for rGO/α-$Ni(OH)_2$ evidences the removal of oxygen containing functionalities of GO and restoration of extended conjugation.[37,38] The atomic percentage of the carbon and nickel in the hybrid material was found to be 56% and 14%, respectively.

The morphology and composition of the hybrid rGO/α-$Ni(OH)_2$ was examined by TEM, FESEM and EDS measurements. The TEM image shows that α-$Ni(OH)_2$ has plate or layer structure over the rGO sheets (Figure 3). The magnified image suggests the stacking of layer-like α-$Ni(OH)_2$ in between the rGO sheets. The selected area electron diffraction (SAED) patterns shown in Figure 3B and Figure 3C were obtained from the encircled region of the materials and the hexagonal spotty pattern confirms the presence of single crystalline hexagonal phase. The SAED pattern in Figure 3B inset indicates that the hybrid material is actually composed of rGO and $Ni(OH)_2$. The atomic percentage of C and Ni in the hybrid material was further obtained from EDS measurement and was 61 and 12 %, respectively, which is in close agreement with the XPS analysis. The EDS line scale analysis further reveals the stacking of α-$Ni(OH)_2$ layer over the rGO sheets (Figure S2). The TEM image of free α-$Ni(OH)_2$ (synthesized in the absence of rGO) shows the growth of wrinkled paper-like morphology (Figure S3). The close examination of the TEM image further suggest the aggregation of layer-like α-$Ni(OH)_2$ in the absence of rGO and have wrinkled morphology. Glucose plays a key role as templates in the growth of layered α-$Ni(OH)_2$. Glucose and in situ generated gluconic acid form hydrogen bond with $Ni(OH)_2$ nuclei formed at the initial stage of the reaction and act as a template in the growth of layer-like structure. Glucose molecules also enable the incorporation of water molecule within the layer and favour the selective growth of α-$Ni(OH)_2$. In the case of the hybrid material, as shown in Scheme 1, the growth of $Ni(OH)_2$ layers actually occurs in between the rGO layers. The in situ generated gluconic

acid and excess glucose present in the reaction mixture actually assist the growth. The possible hydrogen bonding interaction between rGO, glucose/gluconic acid and $Ni(OH)_2$ nuclei formed at the initial stage of the reaction leads to the growth of layered $Ni(OH)_2$ in between the rGO sheets. In order to further ascertain the templating role of glucose, $Ni(OH)_2$ was synthesized in the absence of glucose at identical procedure used for the synthesis of the hybrid material. The TEM image of $Ni(OH)_2$ obtained in the absence of glucose shows the growth of quasi-spherical particles with an average size of 10 nm over the rGO sheets (Figure S4). It confirms that glucose is required as a template for the growth of layer-like structure of α-$Ni(OH)_2$. The XRD measurements show that $Ni(OH)_2$ obtained in the absence of glucose has β phase (Figure S4), implying that glucose has dual role in the synthesis of hybrid material. It favours the controlled and selective growth of layered α-$Ni(OH)_2$. The TGA measurements show that hybrid material is thermally more stable than the free α-$Ni(OH)_2$ and the phase transition of $Ni(OH)_2$ to NiO occurs at high temperature (Figure S5). The electrical conductivity measurements reveal that the hybrid material has higher conductivity (520 Sm^{-1}) than rGO (460 Sm^{-1}).

Electrochemical studies

Figure 4A displays the voltammetric profile of the hybrid material along with rGO, free α-$Ni(OH)_2$ and the physical mixture of rGO and α-$Ni(OH)_2$. Characteristic quasi-reversible redox response corresponding to the redox reaction of α-$Ni(OH)_2$/γ-NiOOH was obtained for all the materials. The close examination of the voltammetric profile reveals that the peak-to-peak separation (ΔE_p) for the hybrid material is much less (<180 mV) than that of free α-$Ni(OH)_2$ (>200 mV) and the physical mixture (>210 mV), suggesting a facile electron transfer. Although both the hybrid material and the physical mixture contain rGO, the ΔE_p value for the hybrid material is ~35 mV less than the physical mixture. The layer-by-layer

arrangement of rGO and α-$Ni(OH)_2$ actually favors the facile electron transfer kinetics. It is known that the area under the voltammogram is proportional to the specific capacitance of the corresponding material. As shown in Figure 4A, the specific capacitance of rGO/α-$Ni(OH)_2$ is higher than the rGO, free α-$Ni(OH)_2$ and the physical mixture. It should be noted here that the performance of the physical mixture is inferior to that of the hybrid material, highlighting the role of layer-by-layer arrangement in the electrochemical activity. As both α-$Ni(OH)_2$ and the rGO sheets are stacked together, the electrolyte can easily permeate to the electrode. The specific capacitance of all the materials was obtained from the discharge experiment at different current density using the following relation:

$$C = I\,\Delta t / \Delta V$$

where I is the discharge current density (A g^{-1}), Δt is the discharge time and ΔV is the potential window. Figure 4C shows the discharge curves obtained for the hybrid material at different current densities. The specific capacitance was calculated to be 1671.67, 1660, 1520, 1339.13 and 1250 F g^{-1} at the current density of 1, 2, 4, 10, and 20 A g^{-1}, respectively. Although capacitance loss was noticed while increasing the current density, the performance of the hybrid material is superior to the free α-$Ni(OH)_2$ and the physical mixture. The specific capacitance of the hybrid material at 1 A g^{-1} is 1.5 to 10 times higher than the other materials (Figure 4B). Moreover, the specific capacitance achieved with the hybrid material is higher than that of the $Ni(OH)_2$- based materials available in the literature (Table S 1). The retention of specific capacitance at high current density of 20 A g^{-1} was 75% with respect to that at 1 A g^{-1}, suggesting that the hybrid material has good capacitive performance (Figure S6A). Such retention of the specific capacitance at high discharge current density can be ascribed to the maximum utilization of electroactive surface of the hybrid material.

It is generally accepted that the internal resistance is one of the important parameters that determine power performance of a supercapacitor. The supercapacitor should have minimum internal resistance in order to deliver high energy in short period of time. Several attempts have been made to reduce the internal resistance using different binders, electrolytes, new active materials, etc.[39] The internal resistance of our hybrid material-based supercapacitor was calculated [40] from the discharge curve shown in Figure 4B and was 0.061 ohm which is 2-3 times lower than the free α-$Ni(OH)_2$ and the physical mixture, further highlighting the excellent performance of the hybrid material. The high electronic conductivity of rGO and the arrangement of α-$Ni(OH)_2$ layers in between rGO sheets actually decreases the internal resistance and enhances the capacitive performance. Although the physical mixture contains electronically conductive rGO, it has significantly high internal resistance. The layer-by-layer arrangement of α-$Ni(OH)_2$ and rGO essentially favors (i) high electron conductivity (ii) large surface availability for the electrolyte and (iii) facile accessibility of α-$Ni(OH)_2$ for the redox reaction. Such layered arrangement favors the easy permeation and facile diffusion of electrolyte ions into the hybrid material. The layered hybrid material behaves like an ''*ion-buffering reservoir*",[41] which actually shortens the OH^- diffusion distance and enhances the Faradaic event even at high current density.

The electrochemical performance of the hybrid material was further examined by electrochemical impedance measurements with frequency ranging from 0.01 Hz to 10^5 Hz at different potentials (Figure 4D). The impedance parameters were obtained by fitting the Nyquist plot using suitable equivalent circuit containing charge transfer resistance (R_{ct}), Warburg impedance (W), double layer capacitance (C_{dl}) and pseudo capacitance (C_{ps}) as the circuit elements (Figure S7). The R_{ct} at the potential of 0.5 V for the hybrid material is 13-23 times lower than that at other potentials. Gradual change in the Warburg line was noticed while increasing the potential. The near linear line along the imaginary axis was observed at

potential of 0.5 V. The deviation from linearity can be ascribed to the pseudocapacitive nature of the material. Highest C_{dl} was obtained at 0.5 V as the low frequency region lies parallel with the imaginary axis. The frequency-dependent specific capacitance was calculated from the Nyquist plot at different potentials and high specific capacitance was obtained at the potential of 0.5 V (Figure S8A).

Retention of the specific capacitance during extensive cycles at higher current density is one of the essential requirements of a supercapacitor. The performance of the hybrid material was further evaluated by examining the life cycle stability. The electrode was subjected to 2000 continuous charge-discharge cycles at a current density of 20 A g^{-1} (Figure 5A). Interestingly, the electrode could retain 81% of the initial capacitance after 2000 charge-discharge cycles (Figure 5B). No loss of capacitance was noticed in the initial 300 cycles and the initial capacitance slightly decreases in the subsequent cycles, presumably due to the change in the volumetric density of α-$Ni(OH)_2$ due to redox process.[42] The 19% loss of specific capacitance after 2000 cycles may be due to the strain in the layered rGO/α-$Ni(OH)_2$ for the diffusion of OH^- ions during continuous charge-discharge cycles. The cyclic performance of free α-$Ni(OH)_2$ and the physical mixture is inferior to that of the hybrid material.

In order to understand the reason for the decrease in the specific capacitance during cycling, we performed post-mortem TEM, XRD and impedance analysis on the electrode material after 1000 extensive cycles. The TEM measurement reveals that although rGO retains its layer, significant deformation of layered α-$Ni(OH)_2$ (Figure 6 A). As shown, the layered $Ni(OH)_2$ breaks into smaller flakes and leached out from the stacked rGO sheets during the extensive charge-discharge cycles at high current density. The α-$Ni(OH)_2$ flakes has an edge length ranging from 5-15 nm. The structural deformation of α-$Ni(OH)_2$ during charge-discharge cycles leads to its leaching from in between the rGO sheets. In contrast, the

post-mortem XRD analysis shows that the $Ni(OH)_2$ retains its original α phase even after extensive cycles (Figure 6B). The close examination of the XRD profile further reveals that the diffraction angle for (001) and (002) planes shifted to higher angle and is very close to the free α-$Ni(OH)_2$. Such shift implies that the α-$Ni(OH)_2$ is not stacked in between the rGO sheets. More importantly, it strongly supports the fact that the α-$Ni(OH)_2$ in the as-synthesized hybrid material is actually stacked in between the rGO sheets. The deformation of layered α-$Ni(OH)_2$ into flakes-like nanostructures actually hinder the facile diffusion of electrolyte ions and hence a loss of specific capacitance. The hybrid material lost its ion buffering ability due to the deformation and leaching out of α-$Ni(OH)_2$ layers from the stacked arrangement. This was further verified by electrochemical impedance measurement and we found ~9 time increase in the R_{ct} value for the hybrid material after the charge-discharge cycles (Figure S9). The increase in the R_{ct} suggests the sluggish charge transport owing to the deformation of α-$Ni(OH)_2$ layers.

The energy storage performance of rGO/α-$Ni(OH)_2$ hybrid material was further evaluated by fabricating a two-electrode asymmetric supercapacitor device (ASD) with rGO and rGO/α-$Ni(OH)_2$ materials (Figure S10). The rGO samples were prepared according to the procedure used for the hybrid material in the absence of nickel precursor. Cyclic voltammetric response in the potential range of 0 – 1.6 V and charge-discharge curves at different current densities for ASD are shown in Figure 7. The broad redox peak corresponds to the redox reaction of pseudocapacitive α-$Ni(OH)_2$. No oxygen evolution peak was noticed during the experiments, highlighting the ideal performance of the device. The specific capacitance was calculated from the charge-discharge curve and was 120, 94, 80 and 44 F/g at a current density of 0.5, 1, 2 and 5A g^{-1}, respectively. The ASD exhibited good recyclability and it retains 100% initial specific capacitance after 500 consecutive charge-discharge cycles (Figure S11). It has an energy density of 42.67 Wh/kg at a power density of

0.4k W/kg and also retains 15.64 Wh/kg at a power density of 4.02 kW/kg. The energy density of ASD is better than that of the other $Ni(OH)_2$-based symmetric and asymmetric supercapacitor devices (Table S2).

Summary

In summary, we have demonstrated a facile non-hydrothermal route for the in situ synthesis of layered hybrid rGO/α-$Ni(OH)_2$ material and the development of supercapacitor electrode. Glucose function as a reducing agent for GO as well as a template for the controlled and selective growth of α-$Ni(OH)_2$. It assist the growth of layered α-$Ni(OH)_2$ in between the rGO sheets. The supercapacitive performance of the hybrid material is superior to that of the free α-$Ni(OH)_2$ and the physical mixture of rGO and α-$Ni(OH)_2$. The ideal integration of α-$Ni(OH)_2$ with rGO actually enhances the overall performance. The large surface area, high electronic conductivity of rGO and facile accessibility of α-$Ni(OH)_2$ to the electrolyte due to layered arrangement facilitate the charge storage process. The hybrid material has very good recyclability; rate capability and it retain 81% of the initial specific capacitance even after 2000 cycles. The performance of the material was further evaluated by fabricating an asymmetric supercapacitor device.

Acknowledgement

This work was financially supported by Department of Science and Technology, New Delhi. SB is a recipient of UGC research fellowship. We gratefully acknowledge DST-FIST for the XRD facility at Department of Chemistry and XPS facility at the Department of Physics, IIT Kharagpur. We also acknowledge Central Research Facility, IIT Kharagpur for TEM and Raman measurements.

References

1. http://science.energy.gov/~/media/bes/pdf/reports/files/ees_rpt.pdf, Basic Research Needs for Electrical Energy Storage: Report of the Basic Energy Sciences Workshop for Electrical Energy Storage. U.S. Department of Energy, Washington, DC, 2007.
2. B. E. Conway. *Electrochemical Supercapacitors: Scientific Fundamentals and Technological Applications*, Kluwer Academic/ Plenum Publisher, New York, 1999.
3. L. L. Zhang and X. S. Zhao, *Chem. Soc. Rev.,* 2009, **38**, 2520.
4. C. Liu, Z. Yu, D. Neff, A. Zhamu, and B. Z. Jang, *Nano Lett.,* 2010, **10**, 4863.
5. H. Wang, H.S. Casalongue, Y. Liang and H. Dai, *J. Am. Chem. Soc*., 2010, **132**, 7472.
6. D. Y. Liu and J. R. Reynolds, *ACS Appl. Mater. Interfaces*, 2010, **2***,* 3586.
7. V. Augustyn, P. Simonbc, B. Dunn, *Energy Environ. Sci.*, 2014, **7**, 1597.
8. J. H. Kim, K. H. Lee, L. J. Overzet and G. S. Lee, *Nano Lett.,* 2011, **11**, 2611.
9. C. Lee, X. Wei, J. W. Kysar and J. Hone, *Science,* 2008, **321**, 385.
10. S. Park and R. Ruoff, *Nat. Nanotechnol.,* 2009, **4**, 217.
11. S. Chen, J. Zhu, X. Wu, Q. Han and X. Wang, *ACS Nano,* 2010, **4**, 2822.
12. H. Huang and X. Wang, *Nanoscale,* 2011, **3**, 3185.
13. C. Zhao, X. Wang, S. Wang, Y. Wang, Y. Zhao and W. Zheng, *Int. J. Hydrogen Energy.,* 2012, **37**, 11846.
14. L. Shen , Q. Che , H. Li , and X. Zhang, *Adv. Funct. Mater.* 2014, **24**, 2630.
15. Z. Wang, X. Zhang, Y. Li, Z. Liu and Z. Hao, *J. Mater. Chem. A,* 2013, **1**, 6393.

16. X. Chen, X. Chen, F. Zhang, Z. Yang and S. Huang, *J. Power Sources,* 2013**, 222**, 326.

17. D. P. Dubal, G. S. Gund, C. D. Lokhande and R. Holze, *ACS Appl. Mater. Interfaces,* 2013, **5**, 2446.

18. S. Yang, X. Wu, C. Chen, H. Dong, W. Hu and X. Wang, *Chem. Commun*., 2012, **48**, 2773.

19. H. Jiang, T. Zhao, C. Li, and J. Ma, *J. Mater. Chem.,* 2011, **21**, 3818.

20. H. B. Li, M. H. Yu, F. X. Wang, P. Liu, Y. Liang, J. Xiao, C. X. Wang, Y. X. Tong, and G. W. Yang, *Nat. Commun*., 2013, **4**, 1894.

21. J. W. Lee, T. Ahn, D. Soundararajan, J. M. Ko and J. D. Kim, *Chem. Commun.,* 2011, **47**, 6305.

22. J. Chang, H. Xu, J. Sun, and L. Gao, *J. Mater. Chem.,* 2012, **22**, 11146.

23. J. T. Zhang, S. Liu, G. L. Pan, G. R. Li and X. P. Gao, *J. Mater. Chem. A*, 2014, **2**, 1524.

24. J. Yan, Z. Fan, W. Sun, G. Ning, T. Wei, Q. Zhang, R. Zhang, L. Zhi and F. Wei, *Adv. Funct. Mater.,* 2012, **22**, 2632.

25. A. Walcarius, *Chem. Mater.,* 2001, **13**, 3351.

26. C. Daniel and J. O. Besenhard, Handbook of Battery Materials, Wiley-VCH, 2011.

27. J. Xie, X. Sun, N. Zhang, K. Xu, M. Zhou, Y. Xie, *Nano Energy,* 2013, **2**, 65.

28. W.S. Hummers and R.E. Offeman, *J. Am. Chem. Soc.,* 1958, **80**, 1339.

29. C. Zhu, S. Guo, Y. Fang and S. Dong, *ACS Nano* 2010, **4**, 2429.

30. X. Fan, W. Peng, Y. Li, X. Li, S. Wang, G. Zhang and F. Zhang, *Adv. Mater*., 2008, **20**, 4490.

31. G.M. Escandar, L.F. Sala and M.G. Sierra, *Polyhedron,* 1994, **13**, 143.

32. P. Warwick, N. Evans, T. Hall and S. Vines, *Radiochim. Acta,* 2003, **91**, 233.

33. D.S. Hall, D.J. Lockwood, S. Poirier, C. Bock and B.R. MacDougall, *J. Phys. Chem. A,* 2012, **116**, 6771.

34. S.R. Shieh and T.S. Duffy, *Phys Rev. B,* 2002, **66**, 134301.

35. S. Stankovich, D. A. Dikin, R. D. Piner, K. A. Kohlhaas, A. Kleinhammes, Y. Jia, Y. Wu, S. B. T. Nguyen and R. S. Ruoff, *Carbon,* 2007, **45**, 1558.

36. J. Liang, R. Ma, N. Iyi, Y. Ebina, K. Takada and T. Sasaki, *Chem. Mater*., 2010, **22**, 371.

37. S. Bag, K. Roy, C.S. Gopinath and C.R. Raj, *ACS Appl. Mater. Interfaces,* 2014, **6**, 2692.

38. R.S. Dey, S. Hajra, R.K. Sahu, C.R. Raj and M.K. Panigrahi, *Chem. Commun.*, 2012, **48**, 1787.

39. M.D. Stoller and R.S. Ruoff, *Energy Environ. Sci.,* 2010, **3**, 1294.

40. H. M. Jeong, J. W. Lee, W. H. Shin, Y. J. Choi, H. J. Shin, J. K. Kang, J. W. Choi, *Nano Lett.,* 2011, **11**, 2472.

41. D. W. Wang, F. Li, M. Liu, G. Q. Lu and H. M. Cheng, *Angew. Chem. Int. Ed*., 2008, **47**, 373.

42. B. Zhao, J. Song, P. Liu, W. Xu, T. Fang, Z. Jiao, H. Zhang and Y. Jiang, *J. Mater. Chem*., 2011, **21**, 18792.

Scheme 1

Scheme illustrating the growth of layered rGO/α-$Ni(OH)_2$ hybrid material.

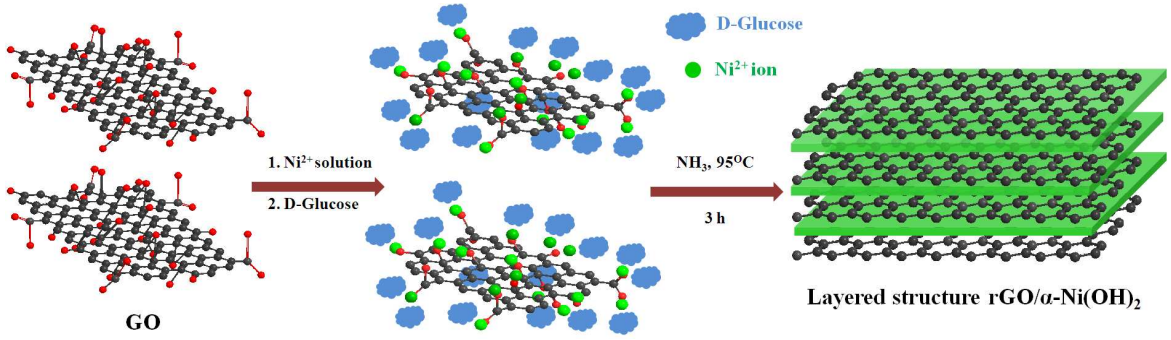

Figure 1

XRD (A) and (B) Raman spectral profiles of (a) GO, (b) rGO, (c) free α-$Ni(OH)_2$ and (d) rGO/α-$Ni(OH)_2$ hybrid material.

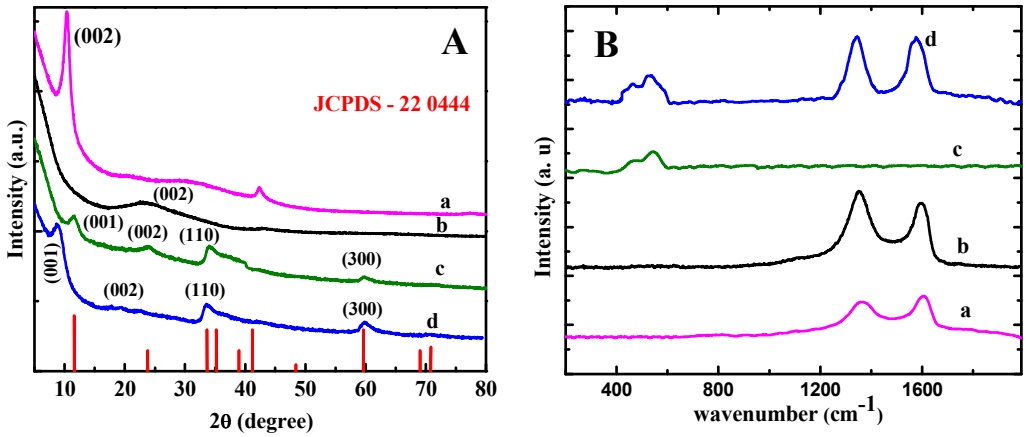

Figure 2

XPS profile of rGO/α-Ni(OH)$_2$ hybrid material and GO. Survey scan (A), Ni 2p (B) and deconvoluted C1s (C) profiles of rGO/α-Ni(OH)$_2$. The deconvoluted C1s spectral profile of GO is shown in (D).

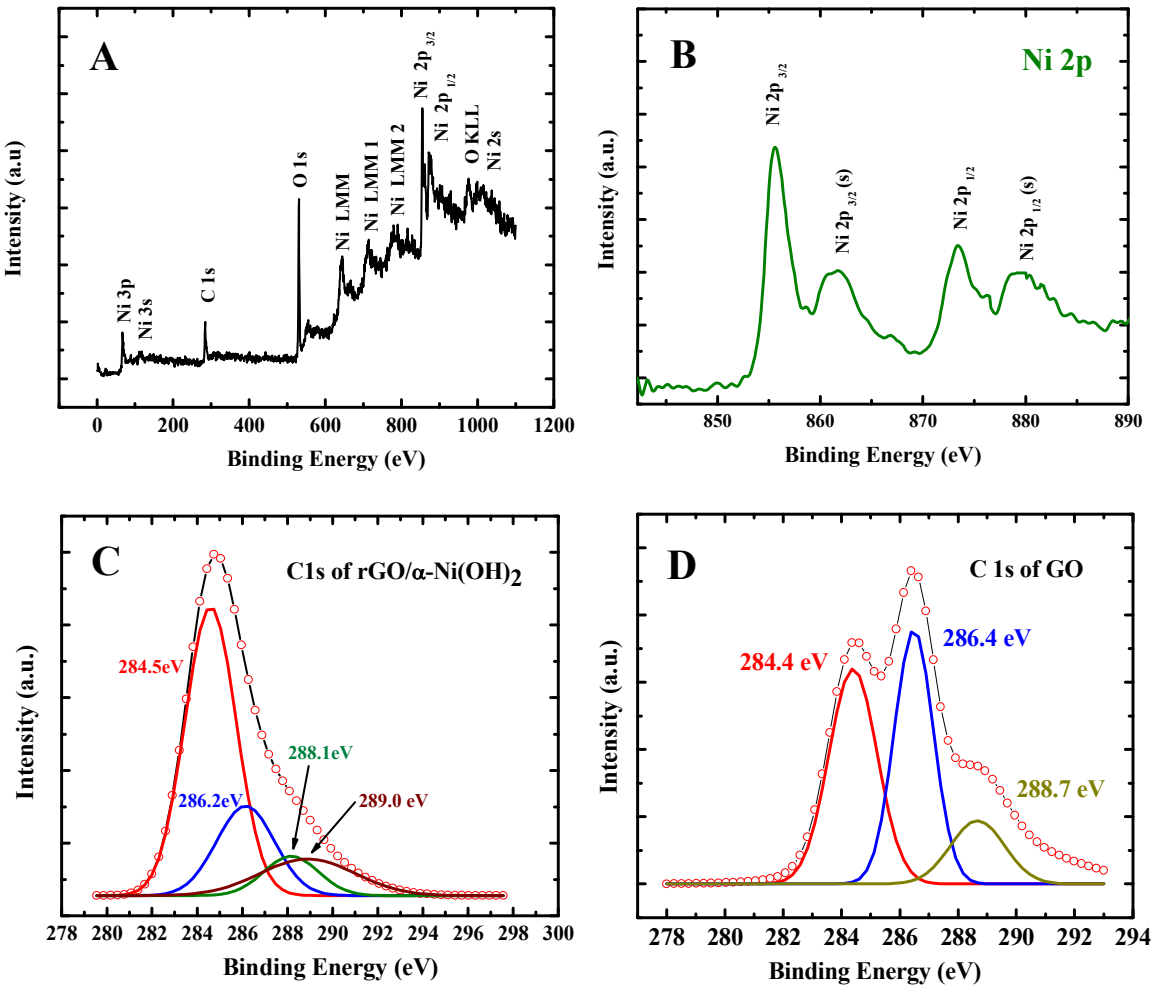

Figure 3

TEM (A, C) and HRTEM (B, D) images of rGO/α-$Ni(OH)_2$ hybrid material. The SAED patterns are given in the inset.

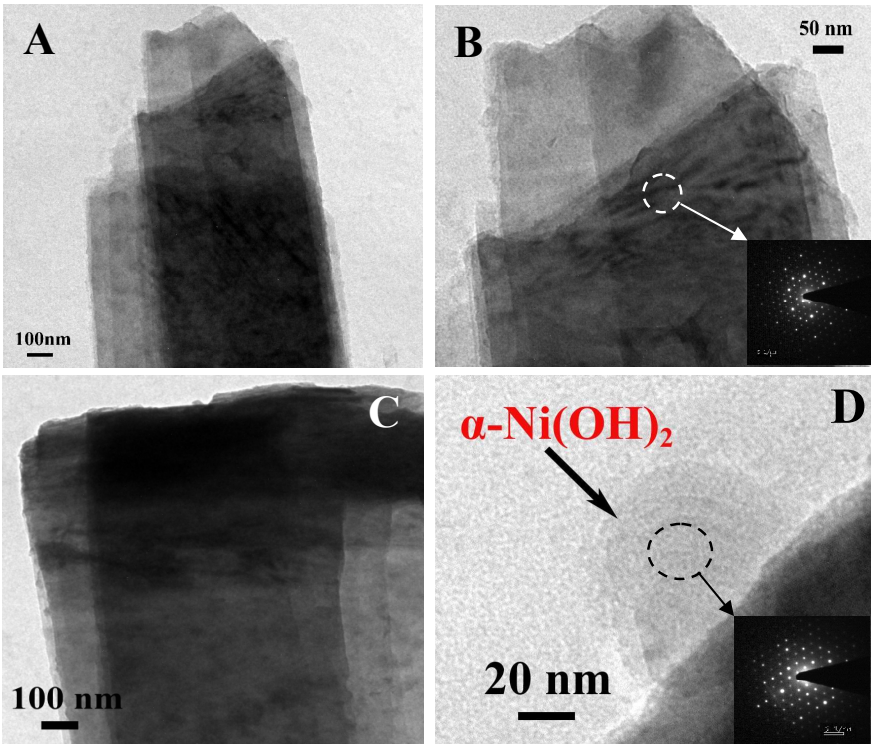

Figure 4

Cyclic voltammograms (A) and discharge profile (B) of (a) rGO, (b) α-$Ni(OH)_2$, (c) physical mixture (d) rGO/α -$Ni(OH)_2$. The discharge profile shown in B was acquired at the current density of $1Ag^{-1}$ whereas in (C) it was obtained for rGO/α-$Ni(OH)_2$ at different current density. (D) Nyquist plot for rGO/α-$Ni(OH)_2$ at different potential.

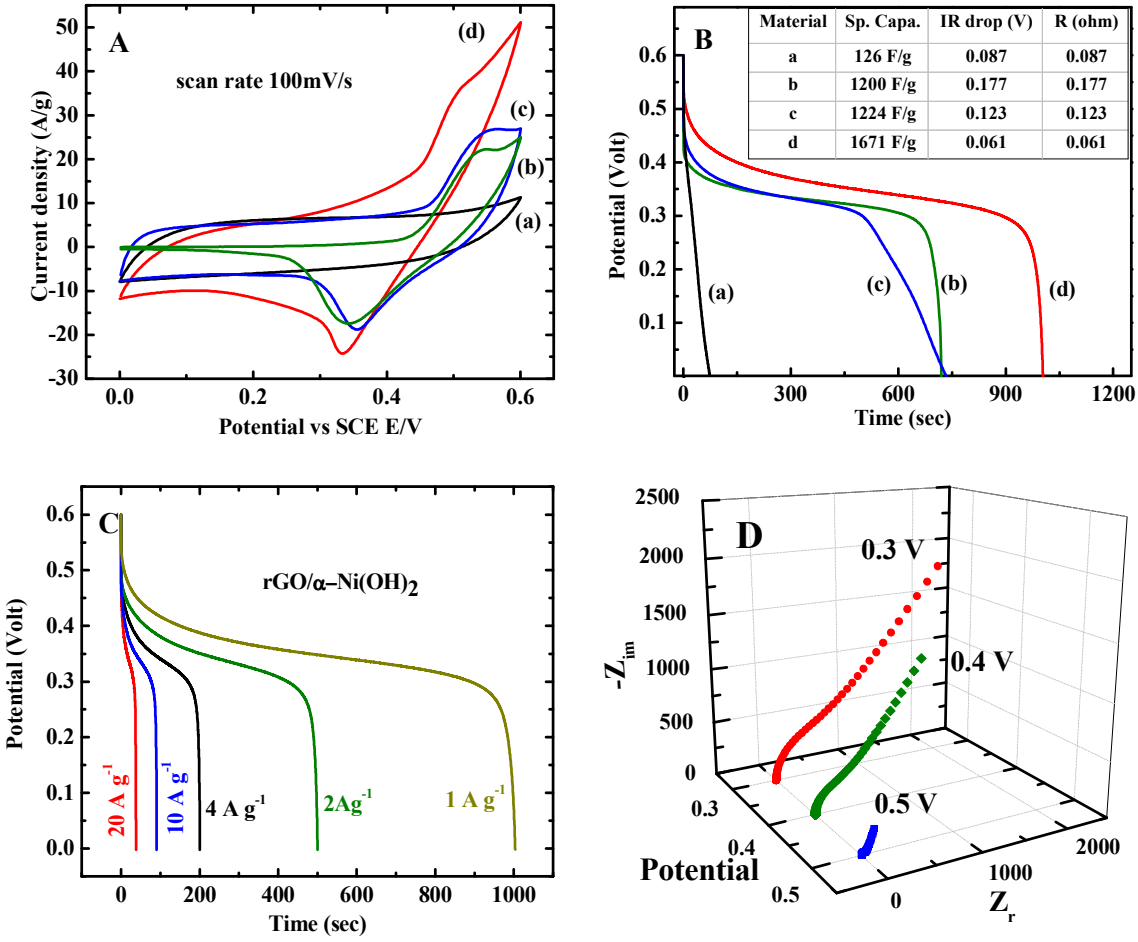

Figure 5.

Charge-discharge profile of rGO/α-$Ni(OH)_2$ (A) and the plot illustrating the retention of specific capacitance during 2000 extensive charge discharge cycles (B).

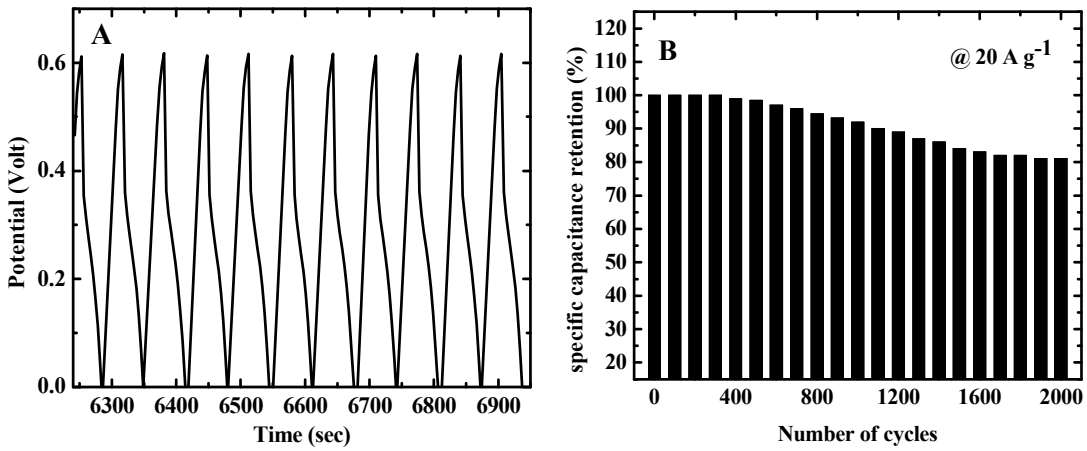

Figure 6.

Post-mortem (A) TEM and (B) XRD analysis of rGO/α-$Ni(OH)_2$. The sample after 1000 charge-discharge cycles has been used in the analysis.

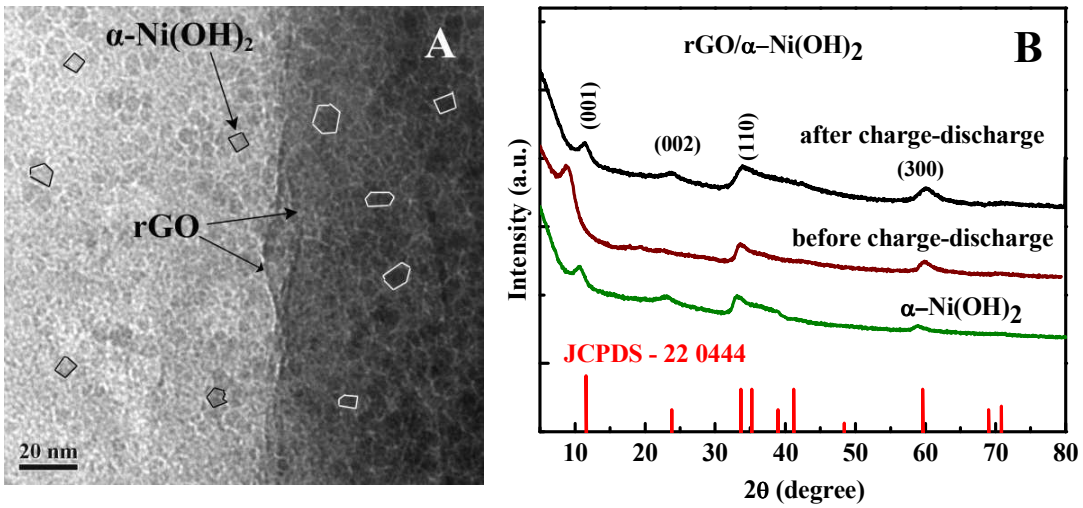

Figure 7.

Cyclic voltammogram at different scan rate (A) and charge-discharge profile at different current density (B) for the asymmetric supercapacitor made of rGO/α-Ni(OH)$_2$ and rGO.

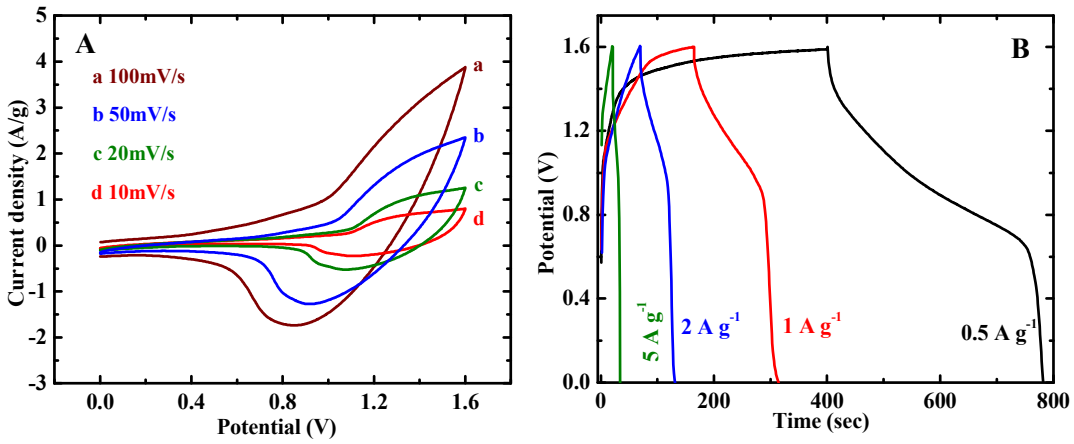

TOC graphics

New method for the synthesis of stacked layered rGO/α-$Ni(OH)_2$ hybrid material with superior supercapacitive performance is demonstrated.